Bioorganic & Medicinal Chemistry 19 (2011) 1790–1801

Contents lists available at ScienceDirect

Bioorganic & Medicinal Chemistry

journal homepage: www.elsevier.com/locate/bmc

Cytotoxic 3,6-bis((imidazolidinone)imino)acridines: Synthesis, DNA binding and molecular modeling

Ladislav Janovec [a], Mária Kožurková [b], Danica Sabolová [b], Ján Ungvarský [a], Helena Paulíková [c], Jana Plšíková [b], Zuzana Vantová [c], Ján Imrich [a,*]

[a] Department of Organic Chemistry, Institute of Chemistry, Faculty of Science, P.J. Šafárik University, Moyzesova 11, SK-04167 Košice, Slovak Republic
[b] Department of Biochemistry, Institute of Chemistry, Faculty of Science, P.J. Šafárik University, Moyzesova 11, SK-04167 Košice, Slovak Republic
[c] Department of Biochemistry and Microbiology, Faculty of Chemical and Food Technology, Slovak Technical University, Radlinského 9, SK-81237 Bratislava, Slovak Republic

ARTICLE INFO

Article history:
Received 17 October 2010
Revised 4 January 2011
Accepted 8 January 2011
Available online 14 January 2011

Keywords:
Proflavine
DNA-intercalation
Antitumor
Topoisomerase
Modeling

ABSTRACT

New acridine derivatives bearing two symmetrical imidazolidinone rings, 3,6-bis((1-alkyl-5-oxo-imidazolidin-2-yliden)imino)acridine hydrochlorides **6a**–**6e** (alkyl = ethyl, *n*-propyl, *n*-butyl, *n*-pentyl, *n*-hexyl), have been prepared and their interactions with calf thymus DNA and selected cell lines were studied. The DNA-binding of **6a**–**6e** to ctDNA was examined by UV–vis, fluorescence, and CD spectroscopy. The binding constants determined by UV–vis spectroscopy were found in the range 1.9×10^5–7.1×10^5 M^{-1}. An electrophoretic separation proved that ligands **6a**–**6e** inhibited topoisomerase I in 40 μM concentration although only those with longer alkyl chains were able to penetrate the membranes and efficiently suppress the cell proliferation. The highest activity in cytotoxic tests was found for 3,6-bis((1-*n*-hexyl-5-oxo-imidazolidin-2-yliden)imino)acridine hydrochloride (**6e**) with IC_{50} = 2.12 μM (HL 60) and 5.28 μM (L1210) after 72 h incubation. Molecular dynamics simulations and calculations of solvent-accessible surface areas (SASAs) were used to explore the intercalation mechanism. MD simulations favor stacking between adjacent C:G base pairs from the minor groove side. MD and SASAs calculations indicate that the decrease of *K* with alkyl extension is due to negative entropic change upon binding.

1. Introduction

The planar acridine scaffold, an important pharmacophore and potent fluorescent ligand intercalating between DNA base pairs, is often used in syntheses of antitumor DNA-targeting drugs.[1–4] Acridine compounds are able to inhibit topoisomerase I and II enzymes, render a DNA damage, disrupt DNA repair and replication, and induce cell death.[5–7] Emerging from our previous studies[8] on the preparation and biological activity of 3,6-bis((3-alkyl-4-oxo-1,3-thiazolidin-2-yliden)imino) acridines **I** (Fig. 1), we decided to improve their DNA-binding and antiproliferative capabilities by replacing the sulfur atom by an amino functionality to obtain new H-bond donor allowing non-bonding interaction between compounds thus obtained and DNA. To study the relation between the structure and lipophilicity, we altered also *n*-alkyl functional groups on the second nitrogen atom of both imidazolidinone rings attached to the acridine core, which are implicated in particular interactions with DNA.

Hence, in this paper we report the synthesis, biochemical properties and cytotoxicity of new proflavine analogs, 3,6-bis-((1-alkyl-5-oxo-imidazolidin-2-yliden)imino)acridine hydrochlorides **6a**–**6e**, as potential anticancer agents. Our study is hoped to shed more light on their DNA binding, human topoisomerase I inhibition, in vitro antiproliferative activity, internalization into cells and resulting DNA fragmentation. On the top, molecular modeling and thermodynamic analysis have further been employed to outline driving forces for intercalation of these compounds into DNA.

2. Results and discussion

2.1. Chemistry

To prepare target bis((imidazolidinone)imino)acridines **6a**–**6e**, starting 3,6-bis(thiourea)acridines **3a**–**3e** were synthesized from commercial proflavine (**1**) via 3,6-di-isothiocyanatoacridine (**2**) by our recent procedure (i, ii, Scheme 1).[8] On this way, a suitable approach to obtain unstable 3,6-bis(carbodiimido)acridine intermediates **5a**–**5e** had to be found, so efficacy of several methods was experienced (Scheme 1). The first one, a direct desulfanation of bis(thioureas) **3a**–**3e** to **5a**–**5e** using dicyclohexylcarbodiimide (iii, a) was not suitable, because of its slow progress. Though analogous reaction of **3a**–**3e** with triphenylphosphine and triethylamine in tetrachloromethane upon reflux (iii, b) was satisfactorily fast and completed within 1 h, a difficult separation of products from by-products precluded its utilization.[9]

* Corresponding author. Tel.: +421 905727892; fax: +421 55 6222124.
E-mail address: jan.imrich@upjs.sk (J. Imrich).

0968-0896/$ - see front matter © 2011 Elsevier Ltd. All rights reserved.
doi:10.1016/j.bmc.2011.01.012

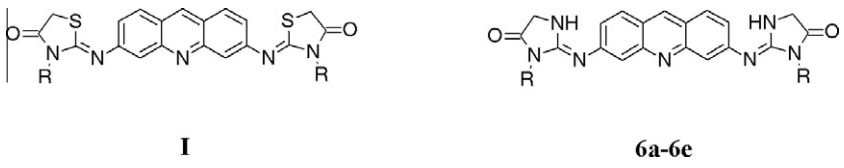

I 6a-6e

Figure 1. Thiazolidinones **I** and acridine bis-imidazolidinones **6a**–**6e**, R = ethyl (a), *n*-propyl (b), *n*-butyl (c), *n*-pentyl (d), *n*-hexyl (e).

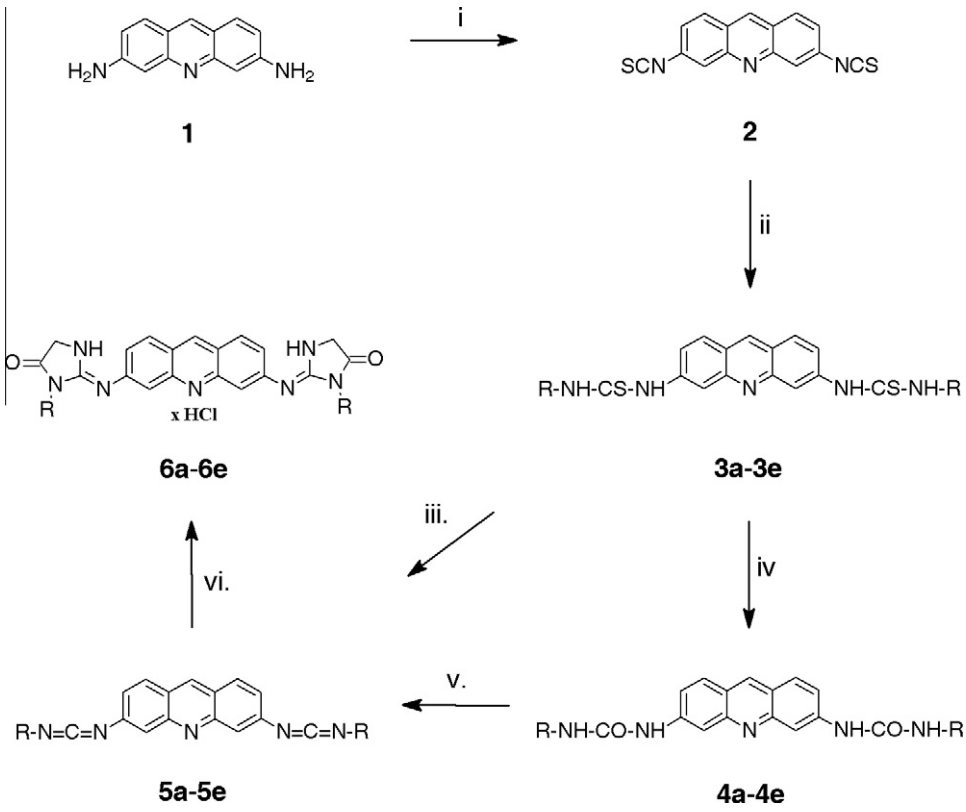

Scheme 1. Reagents and conditions: R = ethyl—**a**; *n*-propyl—**b**; *n*-butyl—**c**; *n*-pentyl—**d**; *n*-hexyl—**e**; (i) $CSCl_2$, $CHCl_3/H_2O$, Na_2CO_3, rt; (ii) RNH_2, CH_3OH, rt; (iii) (a) DCC, THF (dry), reflux; (b) PPh_3, Et_3N, CCl_4, reflux; (c) HgO, Na_2SO_4 (dry), Et_3N, catalytic amount of $CaCl_2$ (dry), THF (dry), 55 °C, 45 min; (iv) MNO, CH_3OH, rt; (v) (a) PPh_3, CCl_4, Et_3N, THF (dry), reflux; (b) DCC, THF (dry), reflux; (vi) ethyl glycinate hydrochloride, Et_3N, THF (dry), then HCl in acetone.

This experience led us finally to a one-pot route in anhydrous tetrahydrofurane using HgO as the desulfanation reagent and then excess of anhydrous Na_2SO_4 as the desiccant. Upon first sight, the reaction seemed to be hopeless again; it proceeded slowly even at 55 °C (ca. 10% conversion in 1 h) and its prolongation diminished the **5a**–**5e** yields by decomposition. However, addition of a large excess of triethylamine together with a catalytic amount of calcium chloride increased surprisingly the rate of the reaction that finished in 45 min (iii, c). The acceleration in this case resulted probably from a thiourea activation in the presence of triethylamine that had eliminated the acidic proton from the thiol form of **3a**–**3e**. The evidence supporting that the presence of a base speeds up the reaction was verified when NaOH was used instead of triethylamine (although then the overall yield of **3a**–**3e** was lowered by fast hydrolysis with NaOH). The role of calcium chloride in this vitalization remains unclear.

Subsequent repeated trials to obtain purified carbodiimides **5a**–**5e** failed because of fast water addition affording corresponding ureas **4a**–**4e** on the adsorbent's surface during TLC monitoring or chromatographic purification. Therefore we utilized **5a**–**5e** immediately in the subsequent step affording **6a**–**6e**. Thus, ethyl glycinate hydrochloride was added to the reaction mixture 1 h after mixing **3a**–**3e** with corresponding reagents (iii, c), and target bis(imidazolidinones) were isolated after overnight stirring and double chromatographic purification as orange solid hydrochlorides **6a**–**6e**, formed using hydrochloric acid in acetone (vi). Overall yields of **6a**–**6e** calculated upon thioureas ranged from 30% to 45%.

Although we have proved the feasibility of an alternative synthetic approach, wherein thioureas **3a**–**3e** and mesitylnitrile oxide were transformed to stable ureas **4a**–**4e** (iv) that subsequently afforded carbodiimides **5a**–**5e** in situ with triphenylphosphine (v, a) or DCC (v, b), this method, as more laborious, was lastly not employed.

2.2. DNA binding studies

The interaction of acridine ligands **6a**–**6e** with calf thymus DNA (ctDNA) was monitored by spectrophotometric titrations in aqueous buffer (see Section 4.3.1.). The UV–vis spectra showed a significant absorption in the range of 350–450 nm, typical for transitions between π-electron energy levels of the acridine ring.[10] Representative titrations are shown in Figure 2.

Along with a significant hypochromism (34–54%) and a partial loss of the fine structure of absorption bands, absorption maxima of all complexes with DNA exhibited bathochromic shifts relative to free ligands, increasing from **6a** to **6e** in the range from 1 to 21 nm (Table 1).

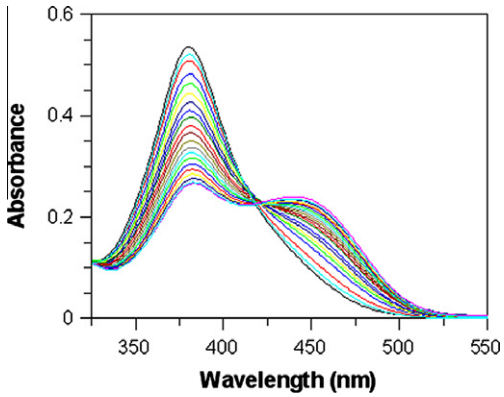

Figure 2. UV–vis spectrophotometric titration of derivative **6b** (25 μM) in 0.01 M Tris buffer (pH 7.4, 24 °C) by increasing concentration of ctDNA (from top to bottom, 0–40 μM bp, at 2 μM intervals).

Table 1
UV–vis absorption data of acridine derivatives **6a**–**6e**

Ligand	λ_{max} free (nm)	λ_{max} bound (nm)	$\Delta\lambda$ (nm)	Hypochromicity (%)
6a	381	382	1	34
6b	381	384	3	54
6c	379	383	4	50
6d	397	405	8	45
6e	399	420	21	47

The addition of DNA to the solution of **6a**–**6e** was typical of one isosbestic point in the spectrum. UV–vis titration data have been used to determine binding constants of ligands **6a**–**6e** with ctDNA using McGhee and von Hippel plots (Section 4.3.2.).[11,12] Binding parameters from spectrophotometric analysis are summarized in Table 2.

Calculated binding constants, *K*, and neighbor exclusion parameters, *n*, clearly indicate a direct link between the intercalation capability and structural changes of bis-imidazolidinones **6**. Large values of binding constants, determined by spectrophotometry in the range from 7.1×10^5 to 1.9×10^5 M^{-1}, prove a high affinity of the acridine ligands to DNA base pairs and correspond to typical binding constants for intercalation complexes between dyes and DNA, found usually in the range 10^4–10^6 M^{-1}. The binding constants for 3,6-bis((imidazolidinone)imino)acridine hydrochlorides **6a**–**6e** with ctDNA are of the same order of magnitude as those found in our previous studies for analogous 3,6-bis(3-*n*-alkylurea)acridine hydrochlorides (alkyl = Et, *n*-Pr, *n*-Bu, *n*-Pen, *n*-Hex) with ctDNA (4.2×10^5–0.9×10^5 M^{-1})[13] and 3,6-bis(3-*n*-alkylthiourea)acridine hydrochlorides (alkyl = Et, *n*-Pr, *n*-Bu, *n*-Pen) with ctDNA (7.6×10^5–2.9×10^5 M^{-1}),[14] and about one order of magnitude greater than those found for 3,6-bis((3-alkyl-4-oxo-1,3-thiazolidin-2-yliden)imino)acridines **I** but with a different DNA type, pUC19 plasmid DNA (6.2×10^4–3.9×10^4 M^{-1}).[8] Observed uniformity of *K* magnitudes validates an assumption that the binding mechanism is heavily dependent on a common structural component of all studied systems, that is, the acridine skeleton, while its lateral substituents, either linear or cyclic, influence binding in a much lesser extent. Such a spectral behavior is generally associated with the intercalation as the dominant binding mode.[13,15]

Depending on the nature of alkyl substituents of both imidazolidinone rings, the binding constants decreased with a growing bulk of alkyls in the order: ethyl > propyl > butyl > pentyl > hexyl (Table 2, Fig. 3).

The same trend has been observed in all of our three former studies.[8,13,14] Clearly, increasing the hydrophobicity of alkyl substituents on the urea, thiourea or heterocyclic systems, which are symmetrically located in the 3,6-positions of the acridine skeleton, impedes the DNA binding and renders the binding energy more positive (Table 2). As modeling this interaction (vide infra, Section 2.7.) suggested a minor groove intercalation to be the dominant mode, we assume that, in addition to acridine itself lying between the DNA base pairs in a nonpolar environment, both alkyl substituents are located, due to the size of the acridin-3,6-disubstituted core, in a more polar surrounding of the DNA grooves where the longer alkyls feel more discomfort than shorter ones inducing thus worsened binding.

In a spectrofluorimetric study (Section 4.3.3.), the free acridine ligands **6a**–**6e** exhibited distinct fluorescence which decreased with an alkyl extension (Table 2). The **6a**–**6e** binding into the DNA helix was separately proven by a significant reduction of their fluorescence upon the addition of DNA to the ligand solution, as depicted on the representative fluorescence spectra of **6b** (Fig. 4). All this evidences a possible usefulness of the title compounds in spectrofluorimetric analysis of biomolecules.

To monitor conformational changes after an addition of ligands **6a**–**6e** to DNA, we used a circular dichroism method (Section 4.3.4.). The complexes produced a CD spectrum typical of B-form DNA with positive and negative Cotton effects at 278 and 245 nm, respectively, (Fig. 5), in accordance with the previous biophysical studies of similar compounds.[13] Changes of negative bands with a non-significant red shift were observed for all compounds. The positive band at 278 nm showed an increase of molar elipticity and mild red shift of the band maxima along with an increase of intensity upon addition of the compounds **6a**–**6e** to DNA but without any clear correlation with the alkyl length. This observation corresponds to a stabilization of the right-handed B-form DNA by the intercalation.

2.3. Topoisomerase I relaxation assay

Topoisomerases are essential DNA-targeting enzymes that initially induce a DNA strand cleavage, and the process is followed by the reorganization and reconnection of the damaged DNA strand. The result of these events is a relaxation of supercoiled DNA, which is required during the transcription or replication. It has been shown that DNA intercalators can significantly interfere with this physiological process.[16–18] The ligand that occupies the

Table 2
Fluorescence data, DNA-binding constants, *K*, neighbor exclusion parameters, *n*, binding free energy, ΔG, and partition coefficients, log *P*, of acridine ligands **6a**–**6e** with ctDNA, determined by UV–vis spectrophotometric titration

Compound	λ_{ex} (nm)	λ_{em} (nm)	F/F_0[a]	K (M^{-1})	n	ΔG (kcal mol^{-1})	Log *P*
6a	381	519	4.43	7.1×10^5	2.2	−8.0	2.17
6b	381	521	5.00	5.7×10^5	2.8	−7.8	3.21
6c	379	521	5.23	4.2×10^5	3.1	−7.7	4.10
6d	379	531	1.00	2.8×10^5	3.8	−7.4	4.99
6e	399	531	1.62	1.9×10^5	4.4	−7.2	5.88

[a] Relative fluorescence intensity of free derivatives **6a**–**6e** (9.7 μM in 0.01 M Tris buffer, pH 7.4, 24 °C) to that of **6d**.

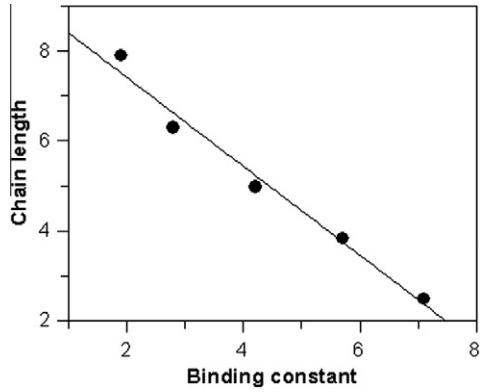

Figure 3. Correlation of chain lengths (Å) of alkyl substituents in acridine derivatives **6a**–**6e** with DNA binding constants ($K/10^5\ M^{-1}$) obtained from spectrophotometry ($k = -0.897$, $r = 0.993$, $S = 0.059$).

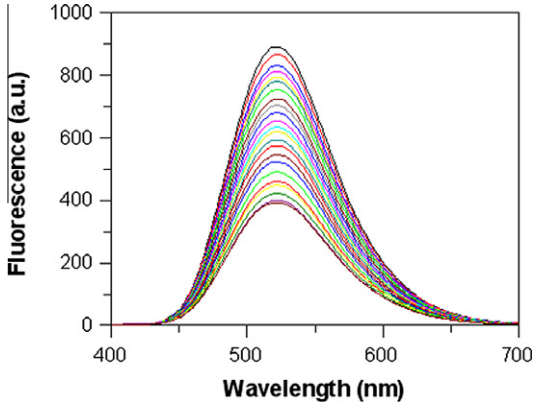

Figure 4. Spectrofluorimetric titration of derivative **6b** (9.7 μM) in 0.01 M Tris buffer (pH 7.4, 24 °C) by increasing the concentration of ctDNA (from top to bottom, 0–100 μM bp, at 2 μM intervals).

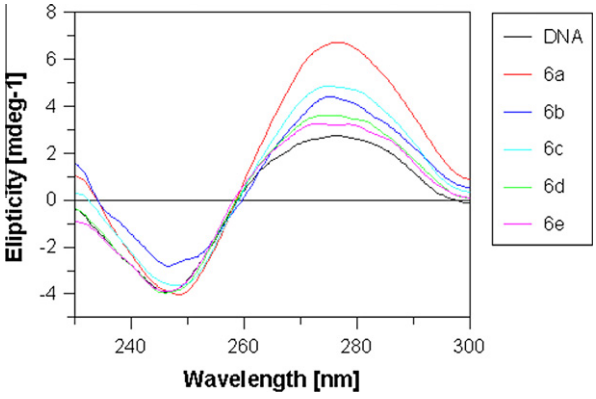

Figure 5. Circular dichroism spectra of ctDNA (1.03×10^{-3} M bp) in the absence and presence of **6a**–**6e** derivatives (1.9×10^{-4} M) in 0.01 M Tris buffer (pH 7.4, 24 °C).

topoisomerase binding site may suppress the association of topoisomerase with DNA, thus influencing the topoisomerase activity. DNA intercalators that inhibit topoisomerase activity or form stabilized ternary complexes with DNA and topoisomerase have a high potential to act as DNA-targeting anticancer drugs.[18,19]

To study the effect of our ligands on the DNA relaxation, supercoiled plasmid pUC19 was incubated with topoisomerase I in the presence of the compounds **6a**–**6e** in concentrations of 5 μM and 40 μM (Section 4.3.5.). As shown in Figure 6, supercoiled DNA was fully relaxed by the enzyme in the absence of **6a**–**6e** (line Topo I). Similarly, a larger fraction of the relaxed form was observed when the ligands **6a**–**6e** were added in the lower concentration of 5 μM (lines $\mathbf{1_a}$–$\mathbf{5_a}$). However, upon increasing the concentration of ligands to 40 μM, the fraction of supercoiled plasmid form exceeded that of the relaxed form (lines $\mathbf{1_b}$–$\mathbf{5_b}$). This observation may result from a topoisomerase I inhibition by the concurrent intercalation of the ligands **6a**–**6e** into a topoisomerase binding site. We assume that the ternary complex consisting of topoisomerase, DNA, and ligand is significantly stabilized under these conditions.

2.4. Cytotoxic effect on human promyelocytic leukemia HL-60 cells and mice leukemia L1210 cells

To determine a cytotoxic potential of the derivatives **6a**–**6e**, we have investigated their antiproliferative effects on human promyelocytic leukemia HL-60 cells and mice leukemia L1210 cells first by a MTT assay (Section 4.3.6., Table 3). As seen from decreasing numbers in columns of Table 3, the cytotoxicity notably increased with the growing length of alkyl side chains: while the bis-ethyl derivate **6a** proved a weak cytotoxic activity against the HL-60 cells and even negligible against the L1210 ones, the most cytotoxic was the most lipophilic bis-*n*-hexyl derivative **6e**.

This observation correlates well with the results of another method—a direct counting of viable cells, obtained using a trypan blue dye exclusion test (Section 4.3.6., Table 4).

The comparison of the present data with the ones from our previous series[8,13,14] proves a close resemblance of the cytotoxic activity of **6a**–**6e** to that of analogous 3,6-bis(3-*n*-alkyl-urea)acridine hydrochlorides[13] towards the HeLa and HCT-116 cell lines in

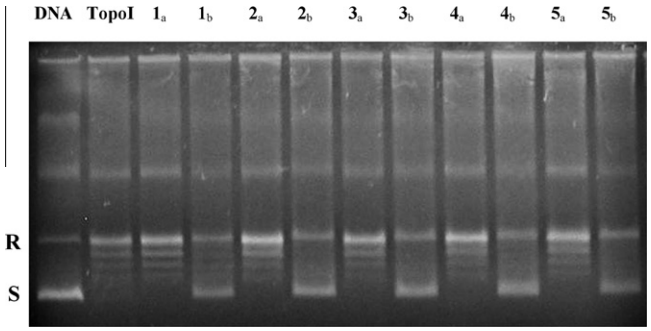

Figure 6. Inhibition of topoisomerase I-induced DNA relaxation by acridine ligands **6a**–**6e**. Native supercoiled pUC 19 (1.4 μg, lane DNA) was incubated for 45 min at 37 °C with 3 units of topoisomerase I in the absence (lane TopoI) or presence of ligands (lane $\mathbf{1_a}$–$\mathbf{5_a}$—5 μM, lane $\mathbf{1_b}$–$\mathbf{5_b}$—40 μM). The DNA samples were run on agarose gel followed by ethidium bromide staining. S = supercoiled plasmid, R = relaxed, open-circular plasmid.

Table 3
Cytotoxicity of **6a**–**6e** derivatives by MTT assay, IC_{50} values

Compound	HL-60[a]		L1210[a]	
	48 h	72 h	48 h	72 h
6a	76.56 ± 3.45	80.28 ± 5.77	>100	>100
6b	74.06 ± 2.86	95.67 ± 7.38	45.83 ± 4.43	68.01 ± 4.98
6c	13.65 ± 1.51	16.35 ± 3.35	29.18 ± 1.67	26.08 ± 5.37
6d	8.37 ± 0.98	8.59 ± 1.97	13.74 ± 1.57	15.25 ± 4.12
6e	4.61 ± 2.08	4.94 ± 2.73	5.52 ± 1.08	5.99 ± 1.00

[a] Cells were incubated without (control) and with 0–100 μM of the tested compounds for 0–72 h. The IC_{50} values (μM) are the concentrations that produced 50 % inhibition of the cell viability. Results are expressed as a mean ± S.D. ($n = 3$).

Table 4
Cell viability by DCC test, IC_{50} values

Compound	HL-60[a]		L1210[a]	
	48 h	72 h	48 h	72 h
6a	83.84 ± 4.12	85.22 ± 5.12	91.74 ± 4.77	>100
6b	70.57 ± 5.23	88.60 ± 5.09	44.67 ± 3.41	65.44 ± 3.70
6c	11.65 ± 2.98	14.65 ± 4.02	26.45 ± 3.98	27.33 ± 2.93
6d	5.31 ± 2.33	7.18 ± 2.98	12.39 ± 3.26	15.68 ± 4.71
6e	2.44 ± 0.29	2.12 ± 0.21	4.31 ± 1.67	5.28 ± 0.76

[a] Cells were incubated without (control) and with 0–100 μM of the tested compounds for 0–72 h. The IC_{50} values (μM) are the concentrations that produced 50% inhibition of the cell viability. Results are expressed as a mean ± S.D. (n = 3).

magnitudes of IC_{50} and the antitumor activity growing with the alkyl extension as well.

A dynamic information on the cytostatic effect of lipophilic bis-*n*-hexyl derivative was obtained from the growth curves of HL-60 human promyelocytic leukemia cells in a 72 h time span. As shown in Figure 7, the derivative **6e** inhibited the proliferation of leukemia cells even at 1 μM concentration, but the compound was toxic in higher concentrations.

2.5. Internalization of acridine derivatives

The cytotoxicity of tested derivatives is associated not only with their DNA-binding properties but may be affected also by their hydrophobicity. An octanol–water partition coefficient, log *P*, was therefore used as a measure of molecular hydrophobicity of the ligands **6a**–**6e** (Section 4.3.7.). The coefficient increased with an extending length of alkyl chains from 2.17 to 5.88 (Table 2). The strongest cytotoxic effect was found for the derivative **6e** having alike the highest hydrophobicity. We have also compared an uptake of the derivatives **6b** and **6e** by the HL-60 cells (Section 4.3.8.). The measurement of their fluorescence after the internalization of the drug showed that accumulation of the compound **6e** in treated cells was substantially higher than that of the compound **6b** (Fig. 8).

The results obtained were also verified by optical and fluorescence microscopy (Section 4.3.9.). An intracellular accumulation of **6b** and **6e** into HL-60 cells was proven through changes of the cells' morphology (Fig. 9). Derivatives **6b** (part A of Fig. 9) and **6e** (part B) were incubated with HL-60 cells for 4 h and 24 h. After 4 h incubation, the fluorescence signal was visible not only in the plasmatic membrane and surroundings, but extended also over the cytosol. Upon prolonged incubation, the differences in a cellular sequestration of these derivatives appeared. The localization of **6b** did not change, however, 24 h after the incubation, the compound **6e** was accumulated also in the nucleus.

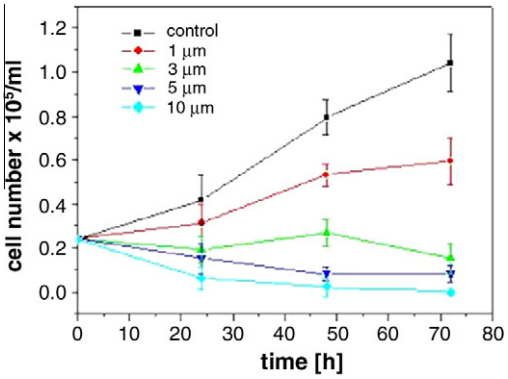

Figure 7. Growth curves of HL-60 cells treated with **6e** for 72 h (concentration range from 1 μM to 10 μM).

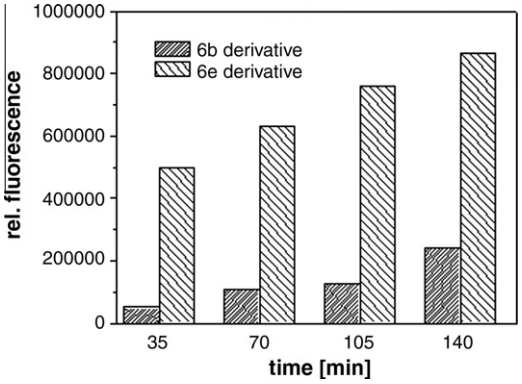

Figure 8. Uptake of compounds **6b** and **6e** into cells. HL-60 cells were incubated with 5 μM concentration of **6b** and **6e** (35, 70, 105 and 140 min), washed with PBS, and monitored by a Typhoon 9210 scanner.

2.6. DNA fragmentation

In addition to characteristic morphology changes, a U937 cells apoptosis induced by the derivatives **6a**–**6e** has been evaluated by an electrophoresis of fragmented DNA (Section 4.3.10., Fig. 10). The U937 cells cultured with the ligands **6a**–**6e** (122 μM) for 18 h exhibited a characteristic DNA ladder pattern of apoptosis. A negligible cleavage of DNA into nucleosomal fragments was observed for the cells treated with **6a**–**6c**. A high uptake rate of the most potent antiproliferative drugs **6d** (*n*-pentyl) and **6e** (*n*-hexyl), characterizing the internalization of the drug, confirmed the drug action.

2.7. Molecular modeling

Acridine bis-imidazolidinones **6a**–**6e**, having two alkyl chains of variable length, may interact with DNA by several modes. To study an energetics of the ligand intercalation, possible groove binding, and base pairs (bp) preferences, we have used, in addition to spectrophotometric determination of binding constants (Table 2), also computational methods as docking (Sections 4.4.1. and 4.4.2.), molecular dynamics simulations (Section 4.4.3.), and thermodynamic parameters calculations (Section 4.4.4.). For docking, ethyl imidazolinone **6a** as a seed compound (free form, not hydrochloride) and two model duplex oligonucleotides, $d[(A:T)]_{10}$ and $d[(C:G)]_{10}$ in the canonical B-form, were chosen to find putative geometries of intercalation complexes. Three modes of intercalation, a major groove intercalation mode, threading intercalation mode, and minor groove intercalation mode have been modeled (Figs. S1–S6 in Supplementary data). The final poses from docking have been used as input coordinates for subsequent molecular dynamics simulations that enabled prediction of preferential intercalation mode among the three postulated above. From overall energetic change upon formation of the complex **6a**–DNA (Table 5) we can see a distinct preference for the minor groove intercalation mode relatively to two other modes, the threading intercalation and major groove intercalation. The preferential minor groove intercalation (Figs. 11 and 12) between A:T bp ($\Sigma\Delta$ = −123.7 kcal mol^{-1}, Table 5) as well as C:G bp ($\Sigma\Delta$ = −207.6 kcal mol^{-1}, Table 5) is documented below. A similar preference of the minor groove intercalation compared to the other modes was observed also from a total energy change, ΔE_{total}, upon the **6a** intercalation into a model oligonucleotide duplex $d[(A:T)]_{10}$ (ΔE = −118.0 kcal mol^{-1}, Table S2, Fig. S3) and a duplex $d[(C:G)]_{10}$: ΔE = −211.5 kcal mol^{-1}, Table S2, Fig. S6).

Consecutively, we have accomplished a thermodynamic analysis of particular energetic contributions to the binding free energy

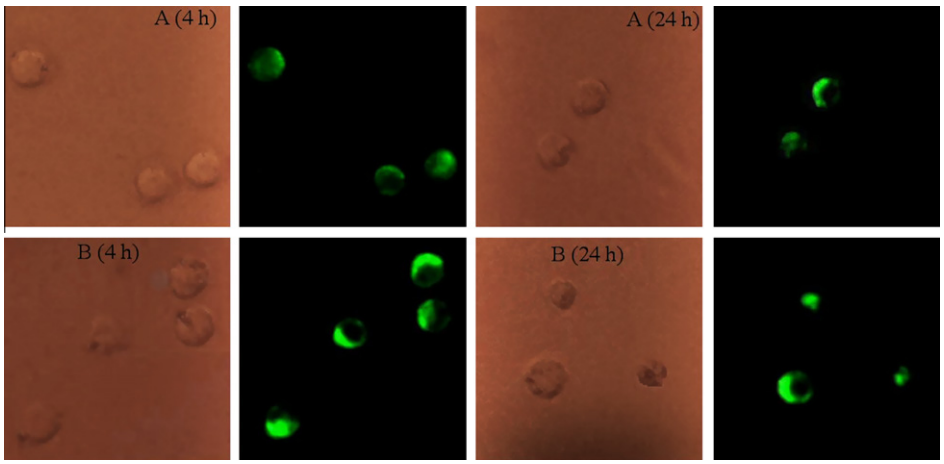

Figure 9. Optical (left) and fluorescence (right) microphotographs of distribution of acridine derivatives in HL-60 cells. The cells were incubated with derivatives **6b** (5 μM, A) and **6e** (5 μM, B) for 4 h (left) and 24 h (right) at 37 °C.

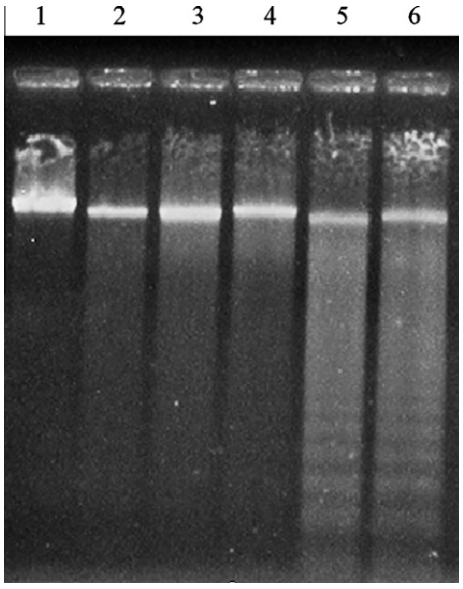

Figure 10. Agarose gel electrophoresis of DNA fragments from cells treated with **6a**–**6e**. U937 cells were incubated with **6a**–**6e** (122 μM) for 18 h. DNA fragmentation was visualized by ethidium bromide after agarose gel electrophoresis. Lane 1—ctDNA, lanes 2–6—cells treated with **6a**–**6e** derivatives, respectively.

of the drug–DNA complex formation (Tables 5, 6, S1, S2 and S3). Generally, this binding free energy can be parsed to contributions of at least five terms[20]

$$\Delta G_{obs} = \Delta G_{conf} + \Delta G_{t+r} + \Delta G_{hyd} + \Delta G_{pe} + \Delta G_{mol},$$

where ΔG_{obs} is the experimentally observed binding free energy, ΔG_{conf} is the free energy contribution from conformational changes in the DNA and drug upon complex formation, ΔG_{t+r} is the free energy cost resulting from the losses in translational and rotational degrees of freedom upon bimolecular complex formation, ΔG_{hyd} is the free energy for the hydrophobic transfer of the drug from solution into its DNA binding site, ΔG_{pe} is the polyelectrolyte contribution arising from the release of condensed counterions from the DNA upon complex formation, and finally, ΔG_{mol} is the free energy contribution from the formation of noncovalent molecular interactions between the drug and DNA like hydrogen bonds, van der Waals and dipole–dipole interactions, etc.. The first term, ΔG_{conf}, has the positive magnitude for the intercalation and near to zero one for the groove binding. The second ΔG_{t+r} term has, by its nature, always positive magnitude, that is, both terms are energetically unfavorable and represent an energy cost. Because any complex formation is characteristic of a free energy decrease, the overall contribution from three remaining terms must decrease the total energy upon binding. Specifically the third, distinctly negative, ΔG_{hyd} term and the fifth ΔG_{mol} term both should act this way.

Table 5
Summary of changes of solvent-accessible surface areas (SASAs), heat capacity (ΔC_p), hydrophobic free energy (ΔG_{hyd}), electrostatic energy (ΔE_{elect}), van der Waals interaction energy (ΔE_{vdw}) for the complex DNA-intercalator **6a** obtained from MD simulations

Complex		ΔA_{np}[b] (Å^2)	ΔA_p[b] (Å^2)	ΔC_p[c] (cal mol^{-1} K^{-1})	ΔG_{hyd}[d] (kcal mol^{-1})	ΔE_{elect}[e] (kcal mol^{-1})	ΔE_{vdw}[f] (kcal mol^{-1})	$\Delta E_{elect} + \Delta E_{vdw}$ (kcal mol^{-1})
d[(A:T)]$_{10}$	*Major*[a]	−350	−56	−127	−10.2	−33.9	−10.4	−44.3
	Threading[a]	−383	−90	−135	−10.8	−53.1	−17.0	−70.1
	Minor[a]	−331	−70	−118	−9.4	−109.4	−14.3	−123.7
d[(C:G)]$_{10}$	*Major*[a]	−264	−60	−94	−7.5	−81.1	−13.9	−95.0
	Threading[a]	−435	−74	−157	−12.6	−94.3	−23.2	−117.5
	Minor[b]	−315	−21	−118	−9.4	−188.3	−19.3	−207.6

[a] Putative mode of intercalation.
[b] Changes of nonpolar (np) and polar (p) SASAs per intercalation calculated using equations $\Delta A_{np} = A_{np}$(complex) − [A_{np}(free DNA) + A_{np}(free ligand)] and $\Delta A_p = A_p$(complex) − [A_p(free DNA) + A_p(free ligand)], resp., from data shown in Table S1.
[c] Calculated using an equation $\Delta C_p = 0.382(\pm0.026)\cdot\Delta A_{np} - 0.121(\pm0.077)\cdot\Delta A_p$.
[d] Calculated from $\Delta G_{hyd} = 80\cdot\Delta C_p$.
[e] Obtained using an equation $\Delta E_{elect} = E_{elect}$ (complex) − [E_{elect} (free DNA) + E_{elect} (free ligand)] from data shown in Table S2.
[f] Obtained using an equation $\Delta E_{vdw} = E_{vdw}$ (complex) − [E_{vdw} (free DNA) + E_{vdw} (free ligand)] from data shown in Table S2.

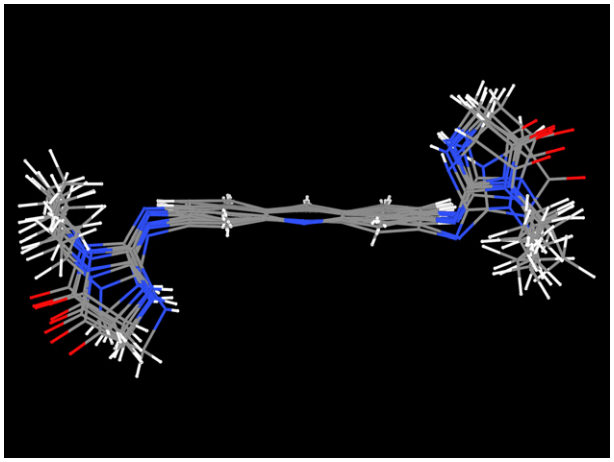

Figure 11. Superposition of dynamic snapshots of ligand **6a**. Coordinates were sampled every 10 ps. Sampling started at 20 ps of full 1 ns production run. Structures were superimposed on the bases of central acridine ring of the first structure. Picture was prepared using Chimera sofware.[23]

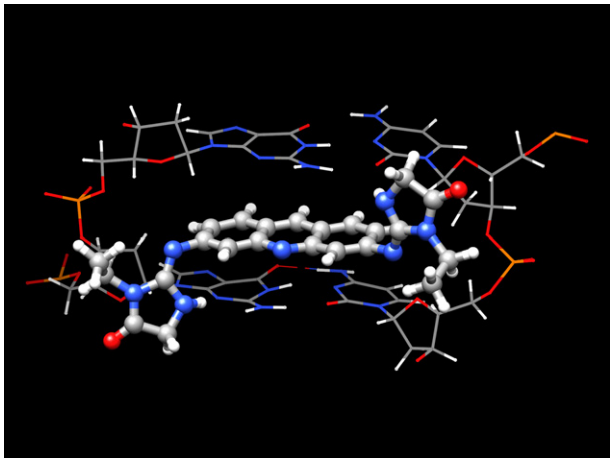

Figure 12. Putative binding of ligand **6a** into adjacent C:G base pairs from minor groove side. View is a cut-out of entire d[(C:G)]$_{10}$. The intercalation cavity with ligand **6a** is visible. Picture was prepared using Chimera software.[23]

Table 6
Summary of changes in solvent-accessible surface areas (SASAs), heat capacities (ΔC_p), and hydrophobic free energies (ΔG_{hyd}) for the complexes d[(C:G)]$_{10}$–**6a–6e** ligands (minor groove intercalation) obtained from docking

	ΔA_{np}[a] (Å^2)	ΔA_p[a] (Å^2)	ΔC_p[b] (cal mol^{-1} K^{-1})	ΔG_{hyd}[c] (kcal mol^{-1})
6a	−370	−40	−137	−10.9
6b	−406	−65	−147	−11.8
6c	−410	−79	−147	−11.8
6d	−477	−65	−174	−13.9
6e	−488	−71	−178	−14.2

[a] Changes of nonpolar (np) and polar (p) SASAs per intercalation calculated using equations $\Delta A_{np} = A_{np}$(complex) − [A_{np}(free DNA) + A_{np}(free ligand)] and $\Delta A_p = A_p$(complex) − [A_p(free DNA) + A_p(free ligand)], resp., from data shown in Table S3.
[b] Calculated using an equation $\Delta C_p = 0.382(\pm0.026)\cdot\Delta A_{np} - 0.121(\pm0.077)\cdot\Delta A_p$.
[c] Calculated from $\Delta G_{hyd} = 80\cdot\Delta C_p$.

To assess the largest ΔG_{hyd} energetic contribution, a useful approximative rule, $\Delta G_{hyd} = 80(\pm10)\cdot\Delta C_p$, where ΔC_p is a heat capacity change of the system upon interaction of the drug with DNA, was published by Record.[21,22] In addition, an empirical relationship which correlates ΔC_p values with the changes of solvent-accessible surface areas (ΔSASAs) upon the complex formation, $\Delta C_p = 0.382(\pm0.026)\cdot\Delta A_{np} - 0.121(\pm0.077)\cdot\Delta A_p$, was derived recently.[22] This equation includes two separate SASA parameters, a nonpolar one, ΔA_{np}, and a polar one, ΔA_p, that both accompany the intercalation process. Thus, the heat capacity change, ΔC_p, of a system of reacting species during the formation of drug–DNA complex, determined either experimentally by isothermal titration calorimetry or from modeling, may be advantageously used to predict the energetic term ΔG_{hyd}.

By an estimation of the SASAs changes (Section 4.4.4.) upon the complexation of the compounds **6a** with model DNA d[(A:T)]$_{10}$ and d[(C:G)]$_{10}$ duplexes, we attempted to selectively determine an influence of hydrophobic forces on the binding of **6a**. The changes of SASAs, ΔA_{np}, and ΔA_p have been calculated using input data either from MD simulations (Table S1) or docking studies (Table S3). The SASAs of free ligands **6a–6e** were obtained from docking studies, the SASAs of free DNA duplexes from MD simulations. Due to a missing input of X-ray data, we have used instead the coordinates calculated by MD simulations. For each putative intercalation mode and the DNA duplex decamer, the coordinates with the lowest total energy have been chosen (Figs. S1–S6). Before application, we have compared our results with known intercalators and found the ΔC_p values close to those derived from crystal structures, for example, for ethidium (−117 cal.mol^{-1} K^{-1}) or propidium (−133 cal mol^{-1} K^{-1}, Table 5, Table S1).[22] This sufficiently validates reliability of our approach to SASAs computations. From calculated changes of SASAs, ΔC_p, and finally ΔG_{hyd} we have found that the highest hydrophobic energy is released when the ligand intercalates into DNA by a threading mode, which represents an entire insertion of the acridine chromophore between the DNA base pairs. The hydrophobic forces are less important for two other intercalation modes, minor groove and major groove, as follows from Table 5. Regarding the base pair type, a threading of **6a** between the d[(C:G)]$_{10}$ bps is more advantageous (−12.6 kcal mol^{-1}, Fig. S5) than between the d[(A:T)]$_{10}$ bps (−10.8 kcal mol^{-1}, Fig. S2).

Clearly, we have observed a contradiction on the intercalation mode predicted by MD versus SASAs calculations. Because MD simulations examine the whole system and involve all energetic contributions, the minor groove intercalation mode calculated by this method should be considered a preferred way of interaction of our ligands with DNA. But this finding means that some of other thermodynamic terms described above must overcompensate the hydrophobic forces that alone would have preferred the threading intercalation. The most important overcompensating factor perhaps should be sought in a MD electrostatic energy term which has by far the largest magnitude for the minor groove intercalation mode as for the C:G bp (−188.3 kcal mol^{-1}, Table 5, Fig. S6) as for the A:T bp (−109.4 kcal mol^{-1}, Table 5, Fig. S3). We assume that this MD term compares the most to $\Delta G_{pe} + \Delta G_{mol}$ terms from the parsed equation.

To disclose an effect of extending alkyl substituents of bis-imidazolidinone ligands **6a–6e** on the binding energetics, we have evaluated how the ΔG_{hyd} hydrophobic term, affordable by SASAs calculations, depends on the alkyl substituents length (Table 6, Section 4.4.4., Table S3). The coordinates for free ligands **6a–6e** and their complexes with d[(C:G)]$_{10}$ were obtained from docking, those for free DNA from MD simulations. From Table 6, an increase of negative ΔG_{hyd} magnitude going from **6a** (−10.9 kcal mol^{-1}) to **6e** (−14.2 kcal mol^{-1}), that is, with a alkyl chain extension, is obvious. This extension induces a systematic reduction of the ligand surface in contact with the solvent. So, the hydrophobic transfer to the binding site to avoid unfavorable hydrophilic interactions in the solution is easier for ligands possessing longer alkyls (Fig. 13). Such a conclusion is furthermore supported by the experimentally obtained neighbor exclusion parameters, *n* (Table 2), whose magnitudes also increase with alkyl extension. It can be

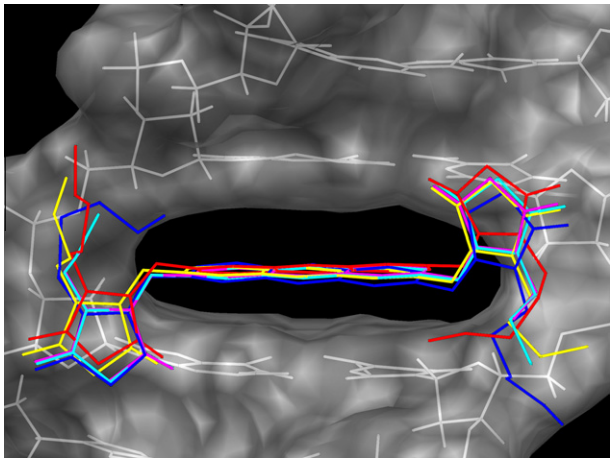

Figure 13. Putative binding modes of all imidazolidinones **6a**–**6e** obtained by docking. Colors of structures: ethyl-purple, propyl–light blue, butyl–yellow, pentyl–red, hexyl–blue, the surface of $d[(C:G)]_{10}$–gray. Nonpolar ligand hydrogens are omitted for clarity. Picture was prepared using Chimera software.[23]

argued that alkyls filling the minor groove render the neighbor base pairs unsuitable for next intercalation. Derivatives with longer alkyls block more space than these with shorter chains.

On the other hand, experimental binding data (Table 2) show that ligands with longer alkyls possess a weaker binding, that is, less negative overall binding free energy, ΔG. Therefore, there should be some factors that compensate more negative ΔG_{hyd} values in the case of large ligands. We assume that ΔG_{hyd} and ΔG_{mol} terms raise upon extending the alkyl length, whereas ΔG_{pe} is small and remains practically unchanged.[20] Longer substituent chains mean a higher energetic gain from the hydrophobic ligand transfer to its binding site (above-calculated negative ΔG_{hyd}), and more non-bonding interactions between enlarged ligand and DNA (presumed negative ΔG_{mol}).

Conversely, ΔG_{conf}, ΔG_{t+r} are both unfavorable free energy contributions representing an energetic cost upon interaction that counteract above-mentioned terms. The ΔG_{conf}, which expresses the cost of intercalation cavity formation, changes probably only little upon the alkyl extension, because the cavity dimensions necessary to accommodate the acridine core inside do not enlarge much going from **6a** to **6e** due to the fact that growing alkyls lie outside of the cavity and their adoption to DNA proceeds without any significant demands on DNA conformational change. The second ΔG_{t+r} term, expressing the loss of translational and rotational degrees of freedom upon bimolecular complex formation, seems to be the most responsible for the observed substituent effects on the experimentally found ΔG trend. The longer alkyl chain, the greater movement restrictions and higher loss of degrees of freedom, that is, a more positive ΔG_{t+r} magnitude. Because $\Delta G_{t+r} = -T{\cdot}\Delta S$ we can conclude that the weaker binding capability versus the alkyl enlargement in **6a**–**6e** follows from an entropic penalty, a large negative entropy change upon binding that becomes yet more negative for ligands with longer substituents, which overcompensates the energy gains from the favorable hydrophobic transfer and the non-bonding interactions in the ligand–DNA complexes.[20]

3. Conclusion

The synthesis of novel 3,6-bis((1-*n*-alkyl-5-oxo-imidazolidin-2-yliden)imino)acridine hydrochlorides **6a**–**6e** (alkyl = Et, *n*-Pr, *n*-Bu, *n*-Pen, *n*-Hex) as fluorescent proflavine analogs, DNA-intercalators, and antitumor substances, was elaborated. The products proved binding constants with calf thymus DNA in the range 1.9×10^5–7.1×10^5 M^{-1} and a higher affinity for C:G base pairs than for A:T ones. The bis-hexyl derivative **6e** showed the highest antitumor effect. On the basis of molecular dynamics simulations and SASAs calculations, the correlation between the alkyl substituent length and the ligand–DNA complex stability has been rationalized as the consequence of entropy decrease upon binding.

From comparison of biochemical and biological properties of **6a**–**6e** under study here with other proflavine analogs examined recently in our laboratory following conclusions on their DNA binding can be drawn:

- The binding constants with ctDNA of bis-imidazolidines **6a**–**6e** were found in the same range 10^4–10^5 M^{-1} as for 3,6-bis(3-alkyl-urea)acridine hydrochlorides[13] and 3,6-bis(3-alkyl-thiourea)-acridine hydrochlorides[14] suggesting that the mechanism of interaction with DNA in all series is analogous by its virtue and just little dependent on the length of alkyls (Et, *n*-Pr, *n*-Bu, *n*-Pen, *n*-Hex) attached to acridine 3,6-positions through the connecting units (urea, thiourea, heterocycle). The data observed correspond to the model of acridine skeleton inserted between DNA base pairs while both alkyl chains accommodate themselves in the minor DNA groove and interact with DNA only by weak non-specific interactions. The smaller (10^4 M^{-1}) binding constants were found for the **I**—plasmid pUC19 interaction.[8]
- Extending the length of alkyls from Et to *n*-Hex brings in all four series an uniform decrease of binding constants roughly one order of magnitude, suggesting a similar mechanism of the substituent effect on the intercalation.
- An antitumor activity towards selected cell lines, IC_{50}, reached μM levels for the most active substances, allowing to consider them to be interesting from the point of further testing. Cytotoxicity against HL-60 cells of the most potent derivative **6e** (2.44 μM, 48 h) is seven-times lower than that of model amsacrine (IC_{50} = 0.34 μM). The antitumor effect of **6e** on L1210 cells (4.31 μM, 48 h) is higher compared to model 9-aminoacridine (45.0 μM) but lower than that of amsacrine (0.05 μM).
- The substituent effect on antitumor activity was dual. With the compounds that do not contain a sulfur atom (bis-imidazolidinones studied here, bis-ureas[13]), the activity increased markedly upon the alkyl extension, while for compounds containing sulfur atom (bis-thioureas[14], bis-thiazolidinones[8]), a reversed trend has been found. This observation is not easy to clarify because the complete mode of action on the intracellular level remains unclear. However, the higher antiproliferative activity of more lipophilic derivatives as pentyl and hexyl could be ascribed to a better cell membrane penetration. Hence, the DNA-binding capability of the compounds under study seems not to be the sole reason of their tumor cell inhibition, but the cellular uptake can also play an important role in the overall pharmacological effect. Moreover, for ligands possessing the thiourea or iminothiazolidinone moiety, a higher electron-withdrawing effect of the sulfur-containing group might increase the acidity of adjacent functionalities—thiourea protons are known to be more acidic than urea protons—and change this way the interaction of ligand's polar parts with DNA.

4. Experimental

4.1. Synthesis

Starting isothiocyanate **2**, thioureas **3a**–**3e** and ureas **4a**–**4e** were prepared according to the published procedures.[8,13,14] Fluorescent yellow solid thioureas **3a**–**3e** were kept in dark under vacuum, otherwise they decomposed turning red. The reactions

were monitored by TLC on Silufol plates at 254 nm. Preparative column chromatography was conducted using a Kiesegel Merck 60 column, type 9385 (grain size 250 nm). ^{1}H (400 MHz) and ^{13}C (100 MHz) NMR spectra were measured on a Varian Mercury Plus NMR spectrometer at room temperature in DMSO-d_6 (Merck) using TMS as an internal standard (0 ppm for both nuclei). Melting points were determined on a Boetius hot-stage apparatus and are uncorrected. Elemental analyses were performed on a Perkin–Elmer CHN 2400 analyzer.

4.1.1. General procedure for the synthesis of 3,6-bis((1-alkyl-5-oxo-imidazolidin-2-yliden)imino)acridine hydrochlorides 6a–6e

Bis-thiourea **3a**–**3e** (0.17 mmol) was suspended in anhydrous THF (3 mL), anhydrous Na_2SO_4 (13 mmol), Et_3N (25 mmol), and a small amount of dried $CaCl_2$ were added, the suspension was stirred at room temperature until turning red, then HgO (7 mmol) was added and intensive stirring continued at 55 °C until thiourea was spent (45 min, TLC monitoring, eluent EtAc/MeOH, 8:1). The precipitate was then filtered off, to the crude THF solution of carbodiimide **5a**–**5e** thus formed ethyl glycinate hydrochloride (3.5 mmol) was added, and the mixture was stirred at room temperature overnight in darkness. With the end of heterocyclization reaction (TLC), the solvent was removed in vacuo, and the residue was purified by the flash chromatography on silica gel, eluent EtAc/MeOH (8:1). The crude product was again dissolved in chloroform and repurified on silica gel, eluent benzene/acetone (3:2), to afford bis-imidazolidine base as a dark-yellow oil. To obtain corresponding hydrochlorides **6a**–**6e**, oils were dissolved in acetone and equimolar portion of 36% HCl in acetone (1:9) was added. Resulting orange precipitate was collected by filtration, washed with acetone, diethyl ether, and dried under vacuum.

4.1.2. 3,6-Bis((1-ethyl-5-oxo-imidazolidin-2-yliden)imino)-acridine hydrochloride (6a)

Yield: 40%. Mp: >100 °C (decomp.). ^{1}H NMR (DMSO-d_6, 400 MHz) δ, ppm 9.54 (s, 1H, 9-H), 8.28 (d, J = 8.8 Hz, 2H, 1-H, 8-H), 7.82 (s, 2H, 4-H, 5-H), 7.51 (d, J = 8.8 Hz, 2H, 2-H, 7-H), 4.05 (s, 4H, 2 × CH_2CO), 3.67 (q, J = 7.2 Hz, 4H, 2 × NCH_2), 1.22 (t, J = 7.2 Hz, 6H, 2 × CH_3). ^{13}C NMR (DMSO-d_6, 100 MHz) δ ppm 171.69 (2 × CO), 157.38 (C-3, C-6), 152.31 (2 × CN), 144.79 (C-9), 141.31 (C-4a, C-10a), 130.89 (C-1, C-8), 125.56 (C-2, C-7), 121.02 (C-8a, C-9a), 107.70 (C-4, C-5), 46.85 (2 × CH_2CO), 38.50 (2 × NCH_2), 12.98 (2 × CH_3). Anal. Calcd for $C_{23}H_{23}N_7O_2$·HCl (465.95): C, 59.29, H, 5.19, N, 21.04. Found: C, 59.38, H, 5.01, N, 20.78.

4.1.3. 3,6-Bis((1-*n*-propyl-5-oxo-imidazolidin-2-yliden)imino)-acridine hydrochloride (6b)

Yield: 45%. Mp: >100 °C (decomp.). ^{1}H NMR (DMSO-d_6, 400 MHz) δ, ppm 9.50 (s, 1H, 9-H), 8.26 (d, J = 8.8 Hz, 2H, 1-H, 8-H), 8.15 (s, 2H, 2 × NH), 7.69 (s, 2H, 4-H, 5-H), 7.44 (d, J = 8.8 Hz, 2H, 2-H, 7-H), 4.04 (s, 4H, 2 × CH_2CO), 3.57 (t, J = 6.0 Hz, 4H, 2 × NCH_2), 1.68 (m, 4H, 2 × CH_2), 0.92 (t, J = 7.6 Hz, 6H, 2 × CH_3). ^{13}C NMR (DMSO-d_6, 100 MHz) δ ppm 171.77 (2 × CO), 157.36 (C-3, C-6), 152.92 (2 × CN), 144.78 (C-9), 141.35 (C-4a, C-10a), 130.84 (C-1, C-8), 125.72 (C-2, C-7), 121.01 (C-8a, C-9a), 107.66 (C-4, C-5), 46.84 (2 × CH_2CO), overlapped (2 × NCH_2), 29.42 (2 × CH_2), 13.44 (2 × CH_3). Anal. Calcd for $C_{25}H_{27}N_7O_2$·HCl (494.00): C, 60.79, H, 5.71, N, 19.85. Found: C, 60.98, H, 5.59, N, 19.74.

4.1.4. 3,6-Bis((1-*n*-butyl-5-oxo-imidazolidin-2-yliden)imino) acridine hydrochloride (6c)

Yield: 46%. Mp: >100 °C (decomp.). ^{1}H NMR (DMSO-d_6, 400 MHz) δ, ppm 9.51 (s, 1H, 9-H), 8.26 (d, J = 8.8 Hz, 2H, 1-H, 8-H), 8.16 (s, 2H, 2 × NH), 7.71 (s, 2H, 4-H, 5-H), 7.44 (d, J = 8.8 Hz, 2H, 2-H, 7-H), 4.04 (s, 4H, 2 × CH_2CO), 3.61 (t, J = 6.8 Hz, 4H, 2 × NCH_2), 1.64 (m, 4H, 2 × CH_2), 1.35 (m, 4H, 2 × CH_2), 0.94 (t, J = 7.2 Hz, 6H, 2 × CH_3). ^{13}C NMR (DMSO-d_6, 100 MHz) δ ppm 171.72 (2 × CO), 157.37 (C-3, C-6), 152.87 (2 × CN), 144.73 (C-9), 141.34 (C-4a, C-10a), 130.83 (C-1, C-8), 125.69 (C-2, C-7), 121.03 (C-8a, C-9a), 107.72 (C-4, C-5), 46.86 (2 × CH_2CO), 38.29 (2 × NCH_2), 29.38 (2 × CH_2), 19.39 (2 × CH_2), 13.53 (2 × CH_3). Anal. Calcd for $C_{27}H_{31}N_7O_2$·HCl (522.05): C, 62.12, H, 6.18, N, 18.78. Found: C, 62.34, H, 6.25, N, 18.63.

4.1.5. 3,6-Bis((1-*n*-pentyl-5-oxo-imidazolidin-2-yliden)imino)-acridine hydrochloride (6d)

Yield: 37%. Mp: >100 °C (decomp.). ^{1}H NMR (DMSO-d_6, 400 MHz) δ, ppm 9.50 (s, 1H, 9-H), 8.26 (d, J = 9.0 Hz, 2H, 1-H, 8-H), 8.16 (s, 2H, 2 × NH), 7.67 (s, 2H, 4-H, 5-H), 7.43 (d, J = 9.0 Hz, 2H, 2-H, 7-H), 4.04 (s, 4H, 2 × CH_2CO), 3.60 (t, J = 6.8 Hz, 4H, 2 × NCH_2), 1.66 (m, 4H, 2 × CH_2), 1.39–1.27 (m, 8H, 4 × CH_2), 0.89 (t, J = 7.2 Hz, 6H, 2 × CH_3). ^{13}C NMR (DMSO-d_6, 100 MHz) δ ppm 171.73 (2 × CO), 157.40 (C-3, C-6), 152.91 (2 × CN), 144.80 (C-9), 141.34 (C-4a, C-10a), 130.87 (C-1, C-8), 125.74 (C-2, C-7), 121.02 (C-8a, C-9a), 107.69 (C-4, C-5), 46.86 (2 × CH_2CO), 38.48 (2 × NCH_2), 28.25 (2 × CH_2), 26.86 (2 × CH_2), 21.63 (2 × CH_2), 13.77 (2 × CH_3). Anal. Calcd for $C_{29}H_{35}N_7O_2$·HCl (550.11): C, 63.32, H, 6.60, N, 17.82. Found: C, 63.49, H, 6.42, N, 17.75.

4.1.6. 3,6-Bis((1-*n*-hexyl-5-oxo-imidazolidin-2-yliden)imino)-acridine hydrochloride (6e)

Yield: 30%. Mp: >100 °C (decomp.). ^{1}H NMR (DMSO-d_6, 400 MHz) δ, ppm 9.50 (s, 1H, 9-H), 8.26 (d, J = 8.6 Hz, 2H, 1-H, 8-H), 8.16 (s, 2H, 2 × NH), 7.68 (s, 2H, 4-H, 5-H), 7.43 (d, J = 8.6 Hz, 2H, 2-H, 7-H), 4.04 (s, 4H, 2 × CH_2CO), 3.59 (t, J = 6.8 Hz, 4H, 2 × NCH_2), 1.65 (m, 4H, 2 × CH_2), 1.35–1.27 (m, 12H, 6 × CH_2), 0.87 (t, J = 7.2 Hz, 6H, 2 × CH_3). ^{13}C NMR (DMSO-d_6, 100 MHz) δ ppm 171.73 (2 × CO), 157.40 (C-3, C-6), 152.90 (2 × CN), 144.78 (C-9), 141.30 (C-4a, C-10a), 130.86 (C-1, C-8), 125.70 (C-2, C-7), 121.01 (C-8a, C-9a), 107.64 (C-4, C-5), 46.85 (2 × CH_2CO), 38.51 (2 × NCH_2), 30.72 (2 × CH_2), 27.14 (2 × CH_2), 25.75 (2 × CH_2), 21.91 (2 × CH_2), 13.81 (2 × CH_3). Anal. Calcd for $C_{31}H_{39}N_7O_2$·HCl (578.16): C, 64.40, H, 6.97, N, 16.96. Found: C, 64.29, H, 6.74, N, 17.21.

4.2. Materials

Propidium iodide (PI), Hoechst 33342, ethidium bromide, Triton X-100, reduced form of glutathione (GSH), 3-(4,5-dimethylthiazol-2-yl)-2,5-diphenyltetrazolium bromide (MTT), dimethylsulfoxide (DMSO), and calf thymus DNA were obtained from Sigma–Aldrich. EDTA, RNase A, and proteinase K were purchased from Serva, plasmid pUC19 (2761 bp, *DH* 5α) and agarose (type II No-A-6877) from Sigma–Aldrich, 5,5-dithio-bis(2-nitrobenzoic acid) (DTNB) from Merck, reduced glutathione and *N*-acetylcysteine from Calbiochem and all other chemicals from Lachema (Czech Republic).

4.3. Biological studies

4.3.1. UV–vis absorption measurements

UV–vis spectra were measured on a Varian Cary 100 UV–vis spectrophotometer in 0.01 M Tris buffer (pH 7.3). The solution of a calf thymus DNA (ctDNA) in TE (Tris–EDTA) buffer was sonicated for 5 min and the DNA concentration was determined from its absorbance at 260 nm. The purity of DNA was determined by monitoring a value A_{260}/A_{280}. DNA concentration measured at 260 nm and expressed as micromolar equivalents of the base pairs ranged from 0 to 40 μM bp. The derivatives **6a**–**6e** were all dissolved in DMSO, from which working solutions were prepared by dilution

using a 0.01 M Tris buffer to concentration 29 μM. All measurements were performed at 24 °C.

4.3.2. Equilibrium binding titration

The binding affinities were calculated from absorbance spectra according to a method of McGhee and von Hippel using data points from a Scatchard plot. The binding data were fitted using a GNU Octave 2.1.73 software.[24]

4.3.3. Fluorescence measurements

Fluorescence measurements of non-bound derivatives **6a**–**6e** were performed on a Varian Cary Eclipse spectrofluorimeter with a 10 nm slit width for excitation and emission beams in the concentration 9.7×10^{-6} M in 0.01 M Tris buffer at pH 7.4. Emission spectra were recorded in the region 400–700 nm using excitation wavelength 379–399 nm. Fluorescence intensities are expressed in arbitrary units. Fluorescence titrations were conducted by the addition of increasing amounts of ctDNA directly into the cell containing solutions of ligands **6a**–**6e** ($c = 9.7 \times 10^{-6}$ M, 0.01 M Tris buffer, pH 7.4, only **6b** titration is depicted in Fig. 4). The concentration range of DNA was 0−100 μM bp. All measurements were performed at 24 °C.

4.3.4. Circular dichroism

CD spectra of complexes ctDNA (1.03×10^{-3} M bp)—ligands **6a**–**6e** (1.9×10^{-4} M) were recorded 10 min after mixing on a J-810 Jasco spectropolarimeter at 24 °C. All measurements were performed in 0.01 M Tris buffer (pH 7.4). A rectangular quartz cell of 1 cm path length was used to obtain the spectra from 200 to 300 nm. Results are presented as a mean of three scans from which the buffer background was electronically subtracted.

4.3.5. Topoisomerase I relaxation assay

For determination of topoisomerase I inhibition activity, calf thymus topoisomerase I (Takara, Japan) and pUC19 DNA (1.4 μg) as the substrate in the reaction buffer (20 μL) containing 0.1% bovine serum albumin (BSA) were used. Appropriate inhibitor was added and the reaction was initiated by the addition of 3 units of topoisomerase I. The reactions were carried out at 37 °C for 45 min. A gel electrophoresis was performed at 7 V/cm for 2 h in TBE (Tris + boric acid + EDTA) buffer on a 0.8% agarose gel. The gel was stained with ethidium bromide (1 mg/ml) and photographed under UV light.

4.3.6. Cytotoxic studies

A cell viability was determined in the presence or absence of tested substances using a MTT microculture tetrazolium assay as described previously.[8,25] The cell proliferation, growth curves, and cytotoxic potential of ligands were determined by a trypan blue dye exclusion test (DCC). For three-day experiments, cells were seeded (1×10^5 cells/mL) in Petri dishes and tested substances (or DMSO–control) were added after 24 h, then cell proliferation was checked after 24, 48, and 72 h. Growth curves were obtained and inhibition concentrations, IC_{50}, were determined. All dye exclusion tests were made three times.

4.3.7. Determination of log *P* values

The log *P* magnitudes for derivatives **6a**–**6e** were obtained using a calculator Marvin 5.1.4 2008 plugins (ChemAxon).[26]

4.3.8. Uptake of 6a–6e into HL-60 cells

Cells harvested in the log phase of growth were counted and seeded in 96-well microtitre plates (2×10^5 cells/240 μL well), treated with non-toxic concentration of **6b**, **6e** (5 μM) and incubated in the dark for 35–140 min. After incubation, the cell cultures were washed and resuspended in 150 μL of PBS. Then, the fluorescence of **6a**–**6e** was measured on a Typhoon 9210 scanner using a 532 nm laser for the excitation of the drug. An ImageQuant software was used for the image display and analysis.

4.3.9. Monitoring of morphological changes

HL-60 cells were seeded (0.5×10^6 mL^{-1}) and treated with **6b**, **6e** (5 μM). After 4 h or 24 h incubation at 37 °C in a humidified atmosphere of 5% CO_2 in air, cells were washed in PBS and observed by an optical microscope and a fluorescence microscope (Axio Zeiss Imager A1, camera AxioCam MRc).

4.3.10. DNA fragmentation

DNA fragmentation in U937 cells was measured after extraction of DNA from a constant number of cells. After the treatment the cell line with **6a**–**6e** for 18 h (37 °C, 5% CO_2), the cells (5×10^5) were collected and washed twice with cold PBS in 500 μL TETlytic solution (10 mM Tris, pH 8.0, 1 mM EDTA, 0.5% Triton X-100), incubated with RNase I (1 mg/mL) for 5 min and then with proteinase K (100 μg/mL) for 30 min at 60 °C. DNA was extracted with NaCl (5 mM) and ethanol (98%) for 60 min at −20 °C. After centrifugation the DNA precipitates were washed with ethanol (70%), resuspended in TE buffer (Tris–EDTA) and separated by electrophoresis on a 1% agarose gel containing ethidium bromide (0.5 μg/mL) and the running buffer TAE (40 nm Tris–acetate, 1 mM EDTA, pH 8.0). The gel was run at 7 V/cm for 2 h and photographed under UV transillumination using an Olympus Camedia 3030 camera.

4.4. Molecular modeling

Molecular models and coordinates for SASAs calculations of acridine ligands **6a**–**6e** were built by the means of building options of GABEDIT package and then minimized using GAMESS software (Ver.: June 6, 1999) at RHF/AM1 semi-empirical level of theory.[27,28] All calculations were carried out in NAMD 2.6 using TIP3P potential for waters, parm99.dat parameters set for nucleic acids, and GAFF atom types for the ligand.[29–33] ANTECHAMBER and XLEAP modules as a part of AMBERTOOLS 1.0 software package were applied to extrapolate missing ligand force-field parameters and derive charges using AM1-BCC method.

4.4.1. Preparation of pseudo-intercalation cavity

The preparation of free $d[(A:T)]_{10}$ and $d[(C:G)]_{10}$ duplexes in a canonical B-DNA form was carried out using GABEDIT program with default parameters. A pseudo-intercalation cavity was constructed by the enlargement of displacement between 5th and 6th bp of DNA to 7 Å and reducing the helix rotation of this part to 10°. In the first round, the DNA was solvated in a water-box, dimensions of which were extended to the distance at least 10 Å from any solute atom. Sodium counterions were then added using XLEAP module to achieve complete neutralization. They were positioned throughout the cell at grid points of negative coulombic potential. Periodic boundary conditions were applied with the particle-mesh Ewans (PME) method, used to treat long-range electrostatic interactions.[34] The entire complex was kept constrained, while allowing the ions and solvent molecule to equilibrate. Resulting system was then equilibrated by 1000-steps of minimization and 20 ps of molecular dynamics at 300 K. The complex was then subjected to 50-steps of conjugate gradient minimization on the whole system to relieve any resulting steric distortion of phosphate backbones in the pseudo-intercalation binding site. The final optimized DNA structures were then extracted and used in subsequent docking computations.

4.4.2. Docking studies

To find a ligand position and orientation, following docking studies were performed: First, the ligand was manually docked

into the DNA cavity to form a minor groove, major groove and threading pseudo-intercalation pose. Docking simulations were carried out using AUTODOCK program ver. 4.0, while MGL TOOLS 1.4.3 was used to prepare the input files.[35–37] United atom representation for the ligand and DNA was used. Gasteiger partial atomic charges for the ligand and DNA were added. The grid for energy was set in the center of ligand with dimensions of 60 points × 60 points × 60 points and spacing of 0.375 Å. Docking runs were performed using Lamarckian genetic algorithm. Docking began with a population of random ligand conformations in a random orientation and at a random translation. Each docking experiment was derived from 200 different runs that were set to terminate after maximum of 2500,000 energy evaluations or 27,000 generations, yielding 200 docked conformations. The population size was set to 150. For other parameters, the default values were used. Coordinates from docking studies were used as input data for SASAs calculations of DNA–ligands **6a**–**6e** complexes (see Section 4.4.4., results in Table S3, Supplementary data).

4.4.3. Molecular dynamics (MD) simulations

Results of docking runs were analyzed using MGL TOOLS 1.4.3 software.[37] The ligand pose with the lowest binding energy of the largest docking cluster was chosen as the final ligand orientation. Nonpolar hydrogens were added and the ligand coordinates were extracted as input parameters for construction of the DNA–ligand intercalation complexes in following molecular dynamics simulations. MD simulations of three intercalation modes of the ligand **6a** insertion into $d[(A:T)]_{10}$ and $d[(C:G)]_{10}$ were performed using the protocol identical with that for pseudo-intercalation structures described above (Section 4.4.1.). This meant 1000-steps of minimization followed by 20 ps equilibrations with constrained solute, and subsequently, 1000-steps of minimization with 200 ps equilibrations for entire system. Finally, full 1 ns MD production run was done. Energy information, averages and coordinates were recorded every 200-steps and non-bonded list was updated every 10-steps. Trajectories were examined visually using VMD 1.8.6 software package.[38] Coordinates from MD were employed as input data for SASAs calculations (see Section 4.4.4., results in Table S1). Averaged energy terms from MD are shown in Table S2 and corresponding snapshoots of the lowest energy are depicted in Figures S1–S6.

4.4.4. Calculation of solvent-accessible surface areas (SASAs)

Solvent-accessible surface areas were determined using the input coordinates from molecular dynamics simulations for both free DNA duplexes, $d[(A:T)]_{10}$ and $d[(C:G)]_{10}$, and complexes DNA–ligand **6a** for all three putative intercalation modes and both DNA duplexes using Tcl module ver. 8.4.1/Tk ver. 8.4.1 of VMD 1.8.6 (Table S1).[22,38] Surfaces of phosphorus atoms, carbon-bound hydrogens and all carbons were classified as nonpolar and those of remaining hydrophilic atoms were defined as polar. Surfaces were generated from coordinates with the lowest total energy obtained from final 1 ns MD production runs with 1.4 Å surrounding radius. The change of the solvent-accessible surface area on binding, ΔA_{total}, is the difference between the area of the complex and the summed surface areas of the free DNA duplex and the free ligand:

$$A_{\text{total}} = A_{\text{np}} + A_{\text{p}}; \qquad \Delta A_{\text{total}} = \Delta A_{\text{np}} + \Delta A_{\text{p}},$$

where A_{np} and A_{p} represent surface contributions from nonpolar and polar atoms, respectively. The binding-induced alterations in component SASAs terms on forming the DNA–ligand complex are thus given by equations:

$$\Delta A_{\text{np}} = A_{\text{np}}(\text{complex}) - [A_{\text{np}}(\text{free DNA}) + A_{\text{np}}(\text{free ligand})],$$

$$\Delta A_{\text{p}} = A_{\text{p}}(\text{complex}) - [A_{\text{p}}(\text{free DNA}) + A_{\text{p}}(\text{free ligand})].$$

For the series of DNA complexes with ligands **6a**–**6e**, SASAs parameters were computed using the intercalation complex coordinates from docking studies as less time-consuming calculations but powerful enough to determine changes of SASAs upon the change of substituents. For similar reasons, only a dominant minor groove intercalation of ligands **6a**–**6e** into sole $d[(C:G)]_{10}$ base pairs was considered. The coordinates of free ligands **6a**–**6e** were obtained using Gabedit and Gamess programs and those of DNA complexes with ligands **6a**–**6e** using AUTODOCK v. 4.0 software with the same protocol as described above (Section 4.4.2.).[35,36] Regarding a rigid DNA receptor geometry, that of $d[(C:G)]_{10}$ from the intercalation complex with **6a**, possessing the lowest total energy after final 1 ns MD production run, was chosen. After docking runs, coordinates of ligand poses with the lowest binding energy were taken and nonpolar hydrogens were added by Chimera software.[23] Such adjusted ligand coordinates were then pasted to $d[(C:G)]_{10}$ receptor geometry file. Resulting complexes were utilized (vide supra) for SASAs calculations (Table S3).

Acknowledgements

Financial support from the Slovak Grant Agency VEGA (grants 1/0053/08, 1/0476/08, 1/0097/10), the State NMR Program (grant No. 2003SP200280203) and The Internal Grant Program of the P.J. Šafárik University in Košice (VVGS No. 7/09-10) are gratefully acknowledged. Molecular graphics images were produced using UCSF Chimera package from the Resource for Biocomputing, Visualization, and Informatics at the University of California, San Francisco (supported by NIH P41 RR-01081). Prof. Pavol Kristian is thanked for valuable advices on the synthesis of **6a**–**6e**.

A. Supplementary data

Supplementary data associated with this article can be found, in the online version, at doi:10.1016/j.bmc.2011.01.012.

References and notes

1. Denny, W. A. *Curr. Med. Chem.* **2001**, *8*, 533.
2. Kapuriya, N.; Kapuriya, K.; Zhang, X.; Chou, T.-Ch.; Kakadiya, R.; Wu, Y.-T.; Tsai, T.-H.; Chen, Y.-T.; Lee, T.-Ch.; Shah, A.; Naliapara, Y.; Su, T.-L. *Bioorg. Med. Chem.* **2008**, *16*, 5413.
3. Desbois, N.; Gardette, M.; Papon, J.; Labarre, P.; Maisonial, A.; Auzeloux, P.; Lartigue, C.; Bouchon, B.; Debiton, E.; Blache, Y.; Chavignon, O.; Teulade, J.-P.; Maublant, J.; Madelmont, J.-P.; Moins, N.; Chezal, J.-M. *Bioorg. Med. Chem.* **2008**, *16*, 7671.
4. Oppegard, L. M.; Ougolkov, A. V.; Luchini, D. N.; Schoon, R. A.; Goodell, J. R.; Kaur, H.; Billadeau, D. D.; Ferguson, D. M.; Hiasa, H. *Eur. J. Pharmacol.* **2009**, *602*, 223.
5. Belmont, P.; Bosson, J.; Godet, T.; Tiano, M. *Anticancer Agents Med. Chem.* **2007**, *7*, 139.
6. Bacherikov, V. A.; Chang, J.-Y.; Lin, Y.-W.; Chen, Ch.-H.; Pan, W.-Y.; Dong, H.; Lee, R.-Z.; Chou, T.-Ch.; Su, T.-L. *Bioorg. Med. Chem.* **2005**, *23*, 6513.
7. Vispé, S.; Vandenberghe, I.; Robin, M. *Biochem. Pharmacol.* **2007**, *73*, 1863.
8. Janovec, L.; Sabolová, D.; Kožurková, M.; Paulíková, H.; Kristian, P.; Ungvarský, J.; Moravčíková, E.; Bajdichová, M.; Podhradský, D.; Imrich, J. *Bioconjug. Chem.* **2007**, *18*, 93.
9. Appel, R.; Kleinstück, R.; Zien, K. D. *Chem. Ber.* **1971**, *104*, 1335.
10. Sabolová, D.; Kožurková, M.; Kristian, P.; Danihel, I.; Podhradský, D.; Imrich, J. *Int. J. Biol. Macromol.* **2006**, *38*, 94.
11. McGhee, J.; von Hippel, P. *J. Mol. Biol.* **1974**, *86*, 469.
12. Jenkins, T. C. In *Methods in Molecular Biology*; Fox, K. R., Ed.; Humana Press: Totowa, New Jersey, 1997; Vol. 90, pp 195–218.
13. Kožurková, M.; Sabolová, D.; Janovec, L.; Mikeš, J.; Kovaľ, J.; Ungvarský, J.; Fedoročko, P.; Kristian, P.; Imrich, J. *Bioorg. Med. Chem.* **2008**, *16*, 3976.
14. Vantová, Z.; Paulíková, H.; Sabolová, D.; Kožurková, M.; Sucháňová, M.; Janovec, L.; Kristian, P.; Imrich, J. *Int. J. Biol. Macromol.* **2009**, *45*, 174.
15. Duff, M. R.; Tan, W. B.; Bhambhani, A.; Perrin, B. S.; Thota, J.; Rodger, A.; Kumar, C. V. *J. Phys. Chem. B* **2006**, *110*, 20693.
16. McClendon, A. K.; Osheroff, N. *Mutat. Res.* **2007**, *623*, 83.
17. Pommier, Y.; Pourquier, P.; Fan, Y.; Stumberg, D. *Biochim. Biophys. Acta, Gene Struct. Expression* **1998**, *1400*, 83.
18. Pommier, Y. *Nat. Rev. Cancer* **2006**, *6*, 789.
19. Basili, S.; Basso, G.; Faccio, A.; Granyhan, A.; Ihmels, H.; Moro, S.; Viola, G. *ChemMedChem* **2008**, *3*, 1671.

20. Chaires, J. B. *Biopolymers* **1997**, *44*, 201.
21. Record, M. T., Jr.; Ha, J.-H.; Fisher, M. A. *Methods Enzymol.* **1991**, *208*, 291.
22. Ren, J.; Jenkins, T. C.; Chaires, J. B. *Biochemistry* **2000**, *39*, 8439.
23. Pettersen, E. F.; Goddard, T. D.; Huang, C. C.; Couch, G. S.; Greenblatt, D. M.; Meng, E. C.; Ferrin, T. E. *J. Comput. Chem.* **2004**, *25*, 1605.
24. Buša, J. In *Octave*; Technical University in Košice: Košice, 2006; Vol. 1,
25. Carmichael, J.; DeGraff, W. G.; Gazdar, A. F.; Minna, J. D.; Mitchell, J. B. *Cancer Res.* **1987**, *47*, 936.
26. http://www.chemaxon.com.
27. http://gabedit.sourceforge.net/.
28. Schmidt, M. W.; Baldridge, K. K.; Boatz, J. A.; Elbert, S. T.; Gordon, M. S.; Jensen, J. H.; Koseki, S.; Matsunaga, N.; Nguyen, K. A.; Su, S. J.; Windus, T. L.; Dupuis, M.; Montgomery, J. A. *J. Comput. Chem.* **1993**, *14*, 1347.
29. Phillips, J. C.; Braun, R.; Wang, W.; Gumbart, J.; Tajkhorshid, E.; Villa, E.; Chipot, C.; Skeel, R. D.; Kale, L.; Schulten, K. *J. Comput. Chem.* **2005**, *26*, 1781.
30. Jorgensen, W. L.; Chandrasekhar, J.; Madura, J.; Klein, M. L. *J. Chem. Phys.* **1983**, *79*, 926.
31. Wang, J.; Cieplak, P.; Kollman, P. A. *J. Comput. Chem.* **2000**, *21*, 1049.
32. Wang, J.; Wang, W.; Kollman, P. A.; Case, D. A. *J. Mol. Graphics Modell.* **2006**, *25*, 247.
33. Wang, J.; Wolf, R. M.; Caldwell, J. W.; Kollman, P. A.; Case, D. A. *J. Comput. Chem.* **2004**, *25*, 1157.
34. Darden, T.; York, D.; Pedersen, L. *J. Chem. Phys.* **1993**, *98*, 10089.
35. Huey, R.; Morris, G. M.; Olson, A. J.; Goodsell, D. S. *J. Comput. Chem.* **2007**, *28*, 1145.
36. Morris, G. M.; Goodsell, D. S.; Halliday, R. S.; Huey, R.; Hart, W. E.; Belew, R. K.; Olson, A. J. *J. Comput. Chem.* **1998**, *19*, 1639.
37. Sanner, M. F. *J. Mol. Graphics Modell.* **1999**, *17*, 57.
38. Humphrey, W. F.; Dalke, A.; Schulten, K. *J. Mol. Graphics* **1996**, *14*, 33.